Complete and incomplete fusion of ^{9}Be + ^{169}Tm, ^{187}Re at near-barrier energies

Y. D. Fang,[1,*] P. R. S. Gomes,[2,†] J. Lubian,[2] M. L. Liu,[1] X. H. Zhou,[1] D. R. Mendes Junior,[2] N. T. Zhang,[1] Y. H. Zhang,[1] G. S. Li,[1] J. G. Wang,[1] S. Guo,[1] Y. H. Qiang,[1] B. S. Gao,[1,3] Y. Zheng,[1] X. G. Lei,[1] and Z. G. Wang[1,3]

[1]*Institute of Modern Physics, Chinese Academy of Sciences, Lanzhou 730000, People's Republic of China*

[2]*Instituto de Física, Universidade Federal Fluminense, Avenida Litoranea s/n, Gragoatá, Niterói, Rio de Janeiro, 24210-340, Brazil*

[3]*Graduate University of Chinese Academy of Sciences, Beijing, 000049, People's Republic of China*

(Received 22 August 2014; published 14 January 2015)

We report the results of the measurements of complete and incomplete fusion of the ^{9}Be + ^{169}Tm and ^{187}Re systems at energies close to the Coulomb barrier. The activation technique with the detection of offline gamma rays was used to derive the cross sections. By comparing the experimental cross sections with coupled-channel calculations that do not include the breakup channel, we found suppression of the complete fusion of the order of 30% for both systems, at energies slightly above the barrier. This suppression corresponds roughly to the measured incomplete fusion. We also investigate a systematic behavior of the suppression of complete fusion cross sections for ^{9}Be on different targets and we found that it does not depend on the target.

DOI: 10.1103/PhysRevC.91.014608 PACS number(s): 25.60.Gc, 25.70.Hi, 25.70.Mn, 25.70.Pq

I. INTRODUCTION

Fusion cross sections with weakly bound nuclei have been a subject of great interest in the last few years [1–4]. These nuclei have very special features, particularly the radioactive neutron or proton halo nuclei, like ^{6,8}He, ^{11}Li, ^{11}Be, and ^{8}B, which have a much more diffused density than the usual nuclei and a high probability of breakup. However, owing to the very low intensity of radioactive beams, several orders of magnitude lower than those of stable beams, fusion-cross-section data induced by those nuclei are not accurate. On the other hand, despite some particular characteristics of unstable nuclei, the reaction mechanisms involved in collisions of stable and unstable weakly bound nuclei should be similar. For this reason, and also for its intrinsic interest, fusion cross sections in collisions of stable weakly bound nuclei, particularly ^{6,7}Li and ^{9}Be, have been investigated, both theoretically and experimentally. The basic question on this subject is whether fusion at near-barrier energies is enhanced or suppressed due to those features and the breakup process.

The answer is not simple, since the fusion process induced by weakly bound nuclei are influenced by several factors [5]. The first one to be considered is the static enhancement effect, since those nuclei have tails of their nuclear densities spreading out of the region that would be occupied by tightly bound nuclei. As a consequence of that, the fusion barrier heights are lower and the resulting fusion cross sections are larger than would be were all nucleons tightly bound. A second effect is the dynamical suppression of the fusion, as a consequence of the couplings with the breakup channel, which leads to an attenuation of the incident current, populating the continuum in an irreversible way to the fusion process. This effect suppresses the fusion cross section, especially at above-barrier energies. However, one may also have dynamical enhancement of subbarrier fusion, similarly to the case of tightly bound system, due to the couplings among bound channels which leads to lower barriers.

Another characteristic of reactions with weakly bound nuclei is the complexity of the large number of possible reaction processes. Figure 1 shows, as an example, reaction mechanisms in collisions of the stable weakly bound ^{9}Be nucleus. This nucleus may break up into neutron plus ^{8}Be, with breakup energy of 1.67 MeV, and the latter is unstable and decays into two alpha particles after a typical half-life of the order of 10^{-16} seconds. Direct and sequential complete fusion cannot be separated experimentally. Also, the noncapture breakup may be prompt breakup, which occurs when the projectile is approaching the target (typically on the order of 10^{-22} seconds), or delayed breakup, which occurs when the projectile has already left the interaction region [6–8]. Figure 2 is a schematic cartoon of prompt and delayed breakups of ^{9}Be. Only the prompt breakup may affect fusion [6–8].

Rafiei *et al.* [6] showed that the cross section of the delayed breakup of ^{8}Be is much larger than that of the prompt breakup of ^{9}Be.

Although it has already been shown [9,10] that the noncapture breakup of ^{6}Li increases with the target mass and charge, some systematic studies of the effect of the breakup on the fusion of ^{6,7}Li on different targets [11–15] have shown that the complete fusion (CF) suppression at energies close but above the barrier is almost target independent. The suppression factor is defined as the dynamic breakup effect on the CF, and it is derived in the comparison of theoretical predictions that do not take into account the breakup couplings. It is important to mention that there are no measurements of CF for light targets, since the residual nuclei from complete fusion and incomplete fusion (ICF), defined as fusion of part of the projectile with the target, coincide for those light systems and, therefore, only total fusion (TF, which is the sum of CF and ICF) can be measured. The reason the suppression is target independent may be the predominance of delayed breakups over prompt breakup, where the former is the sequential breakup following direct transfer of nucleons or breakup following the excitation

*fangyd@impcas.ac.cn; Present address: Research Center for Nuclear Physics, Osaka University, Ibaraki, Osaka 567-0047, Japan.

†paulogom@if.uff.br

 ©2015 American Physical Society

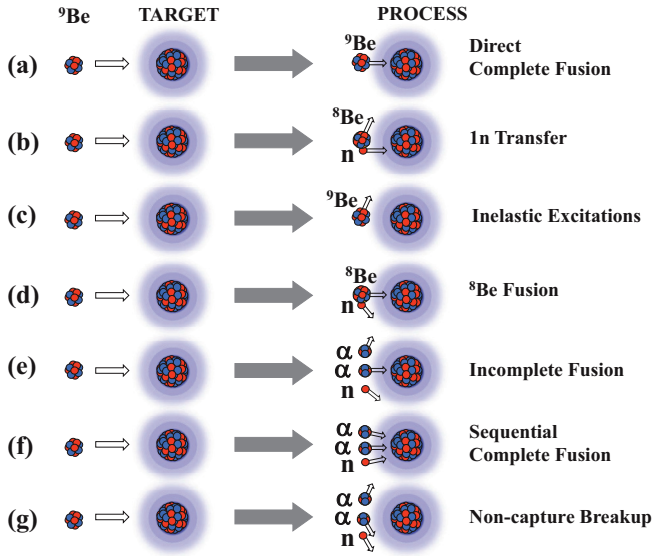

FIG. 1. (Color online) Cartoon showing several different reaction processes which can occur with ^{9}Be as projectile.

of the projectile to a long-lived resonance above the breakup threshold as it traverses the interaction region.

For ^{9}Be the situation is not so clear [13–17]. There are some reported works on the CF of this projectile on different targets, ranging from ^{89}Y to ^{209}Bi [14,18–24], but the suppression factor of the CF at energies slightly above the barrier does not follow a systematic behavior. For lighter targets, like ^{27}Al and ^{64}Zn [25–27] and for ^{238}U [28], only TF cross sections were measured. In order to contribute to the investigation of the dynamical effect of the breakup of ^{9}Be on fusion induced by this projectile, we performed experiments to measure CF and ICF of ^{9}Be on the ^{187}Re and ^{169}Tm targets at energies close to the Coulomb barrier.

In Sec. II we describe the experimental setup. In Sec. III we show the results and describe the cross-section-data reduction. In Sec. IV we compare the experimental fusion cross sections with coupled-channel calculations that do not include the breakup channel. In Sec. V we investigate the possible systematic reached for the suppression of the CF at energies slightly above the barrier. Finally, in Sec. VI we present a summary and some conclusions.

II. EXPERIMENT DETAILS

The cross sections of reaction products formed in the fusion of ^{9}Be + ^{169}Tm and ^{9}Be + ^{187}Re systems at energies around the barrier were measured by using an activation technique. The technique used is based on two main steps: The first step consists of the irradiation of ^{169}Tm and ^{187}Re targets. The second step consists of the offline detection of the γ rays emitted after the electron-capture decay of the evaporation residues (ERs). According to statistical model calculations, most of the ERs associated with CF and ICF reactions produced in ^{9}Be + ^{169}Tm and ^{9}Be + ^{187}Re systems decay mainly by electron capture, with half-lives approximately in the range between 1 hour and 14 days, making the offline γ-counting measurement possible. As we discuss in the following, the analysis of the characteristic γ-ray spectra and/or associated decay curves makes it possible to uniquely identify the ERs and in turn, extracting the cross sections of different ERs. This technique has been widely used in the literature and also has been successfully applied by our group to measure the fusion excitation function of the system ^{9}Be + ^{181}Ta [20].

The experimental procedures associated with the activation of the ^{169}Tm and ^{187}Re targets and the subsequent offline γ-ray measurements are given in the following sections.

A. Activation measurements

The experiments were performed at the sector-focusing cyclotron in the Heavy Ion Research Facility Lanzhou (HIRFL). The experimental setup used in the activation measurements was mounted inside a scattering chamber, as shown in Fig. 3. Two monitor detectors were used to detect the elastically scattered particles from a Au foil placed upstream from the targets. A stack of targets was used to extract the excitation function using the energy-degradation technique. In addition, a Faraday cup was installed downstream of the scattering chamber to measure the beam current.

The typical average thickness of the natural ^{169}Tm targets was around 600 μg/cm^2, while the thickness of ^{187}Re targets (99.6% enriched) was in the range of 310 to 370 μg/cm^2. The thickness of each target was determined by using a microbalance. The targets were prepared by the high-vacuum evaporation technique on Al backing of thickness around

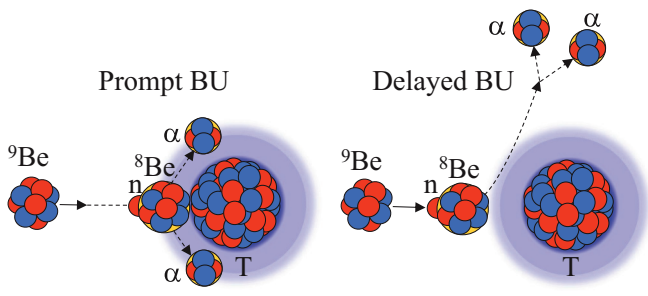

FIG. 2. (Color online) Schematic view of prompt and delayed breakups which can occur with the ^{9}Be projectile. Only prompt breakup may affect fusion.

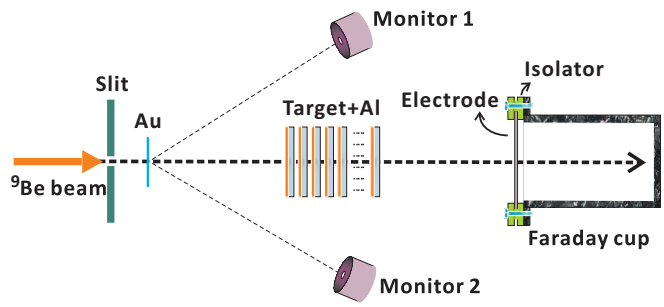

FIG. 3. (Color online) Sketch of the experimental setup for excitation function measurement using the energy-degradation technique.

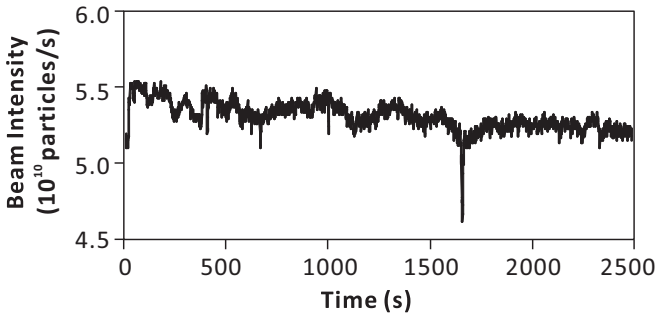

FIG. 4. Beam current as a function of the time.

1.0 mg/cm^2. The Al backing of the targets served as the energy degrader as well as the catcher to trap the recoiling residues produced during irradiations. The initial energy of the ^{9}Be beam was 50.4 MeV. In order to cover a wide energy range for measuring the excitation functions as well as to lower the uncertainty in beam energy, each type of target was grouped into two stacks (each stack contains eight target-Al foils). In the first run, the irradiation of the stack covered the desired energy range of 42 to 50 MeV. For the second run, we used a relatively thick Al foil (11.1 mg/cm^2) placed in front of the stack in order to obtain irradiation at beam energies of 32 to 40 MeV. The mean energy of the ^{9}Be ion beam incident at half the thickness on each target in the stack was calculated from the energy degradation of the incident-beam energy, using ATIMA calculation within the LISE++ program [29,30].

The ^{9}Be beams were collimated by a 3-mm-diameter circular collimator, placed 5 cm upstream from the Au foil. The beam current was maintained in the range of 10 to 15 and 30 to 35 enA, respectively, for the ^{9}Be + ^{169}Tm and ^{9}Be + ^{187}Re systems. The beam flux was determined from the charge collected in the Faraday cup by using a precision current-integrator device, while a negative 400 V bias on the collector repelled the secondary electrons. In addition, two monitors kept $\pm 30^{\circ}$ with respect to the beam direction were used to detect the beam particles. The two sets of values were found to agree with each other. As we discuss in the next sections, to properly reconstruct the production cross sections, it is necessary to know the beam current as a function of time during the irradiation. To this end, the counts of the current-integrator device and two monitor detectors were read by the acquisition every second. As an example, in Fig. 4 we show a typical beam current as a function of the time obtained in the run of the ^{9}Be + ^{187}Re experiment. The irradiation time in the first and second runs were 12 h and 15 h, respectively.

B. Postirradiation measurements

The reaction products, which were stopped in the target and Al backing, were identified by their characteristic γ rays by offline measurements that used a dedicated array consisting of 16 high-purity Ge (HPGe) detectors coupled to a VME-based maximum integrated data acquisition system. After the end of each activation run, the target and its associated catcher were taken from the reaction chamber and were placed in between two HPGe detectors positioned 180° to each

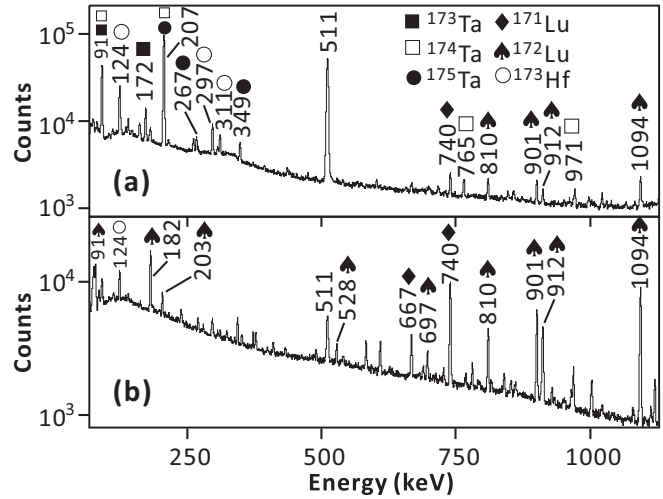

FIG. 5. Offline γ-ray spectra for ^{9}Be + ^{169}Tm system at 47.97 MeV measured at (a) 2 h after the end of the activation with measuring time 2 h, and (b) 5 d after the end of the activation with measuring time 24 h. The γ lines from different reaction products are labeled. The open circles (○) correspond to the decay of ^{173}Hf produced by the decay of its higher-charge isobar precursor ^{173}Ta.

other, where single γ-ray measurements and γ-γ coincidence measurements could be made simultaneously. The offline measurement time was from 12 to 15 hours in duration. The distance between the target and the detector was ~10 cm. The crystal of the detector and the target-Al foils were surrounded by a cylindrical Pb shield to reduce scattered γ rays from neighboring targets and background from natural radioactivity. There are eight identical setups in this array, which could detect the γ rays independently, thus allowed measurements of all the irradiated targets in one stack at a time. The absolute efficiencies of the detectors were determined by using a set of calibrated radioactive sources (^{60}Co, ^{133}Ba, and ^{152}Eu) mounted in the same geometry and absorption conditions as the target-Al foils.

The excited compound nuclei formed in the fusion of ^{9}Be + ^{169}Tm and ^{9}Be + ^{187}Re decay predominantly by neutron evaporation. The dominant channels observed in these two systems both are $3n$, $4n$, and $5n$ evaporation channels. The evaporation residues were identified not only by their characteristic γ-ray energies, but also by their half-lives and branching ratios. A typical γ-ray spectra along with some of the assigned residues populated in ^{9}Be-induced reactions on ^{169}Tm and ^{187}Re at, respectively, 47.97 and 48.13 MeV, are shown in Figs. 5 and 6. The evaporation residues identified by their γ-ray energies (E_{γ}), half-lives ($T_{1/2}$), and branching ratios I_{γ}, etc., are given in Tables I and II, respectively.

III. DATA REDUCTION AND RESULTS

The determination of the experimental ER cross sections from the γ-ray-activity measurements requires knowledge of (a) the total number of nuclei present in the target, (b) the beam current as a function of time during the activation, and (c) the total number of residues produced at the end of irradiation. Given the fact that, during the activation, the

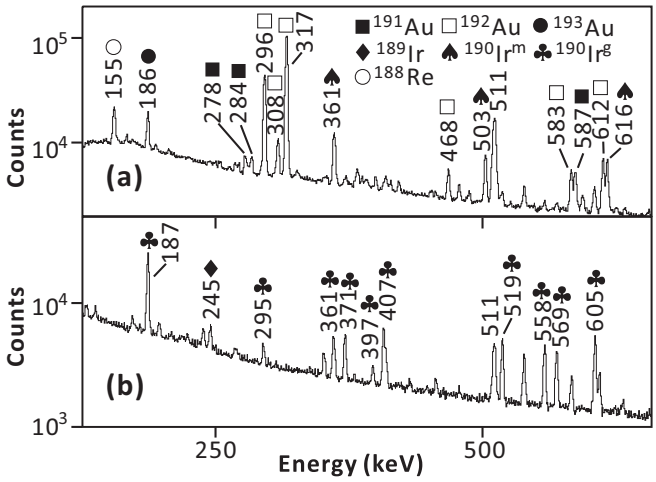

FIG. 6. Offline γ-ray spectra for ^{9}Be + ^{187}Re system at 48.13 MeV measured at (a) 5 h after the end of the activation with measuring time 2 h, and (b) 8 d after the end of the activation with measuring time 24 h. The γ lines from different reaction products are labeled.

population of a given residue competes with its decay, we divided the irradiation time into 1 second steps and used the following expression:

$$\sigma_\gamma(E) = \frac{N_\gamma \lambda}{N_T \varepsilon_\gamma I_\gamma (1 - e^{-\lambda}) S}, \quad (1)$$

where

$$S = \sum_{n=1}^{m} I_n [e^{-\lambda(t_1 - n)} - e^{-\lambda(t_1 + t_2 - n)}]. \quad (2)$$

In Eqs. (1) and (2), t_1 is the time between the beginning of irradiation and the measurement, t_2 is the time of the measurement, N_γ is the yield of the γ line of interest observed in time t_2, λ is the decay constant of the ER, N_T is the total number of nuclei present in the target, ε_γ is the efficiency of HPGe detector at the peak energy, I_γ is the intensity branching ratio of the γ line, I_n is the beam current at the nth step and m is the total number of steps.

The nuclear spectroscopic data used in the evaluation and the measurements of cross sections are given in Tables I and II, respectively, for ^{9}Be + ^{169}Tm and ^{9}Be + ^{187}Re systems. Only

TABLE I. List of identified reaction residues in the ^{9}Be + ^{169}Tm reaction, and their decay data [31,32].

Residue	$T_{1/2}$	J^π	E_γ (keV)	I_γ (%)
^{173}Ta($5n$)	3.14 h	$5/2^-$	160.4	4.9
			172.2	17.5
^{174}Ta($4n$)	1.14 h	3^+	764.8	1.26
			971.1	1.09
^{175}Ta($3n$)	10.5 h	$7/2^+$	266.9	11.2
			348.5	12.0
^{171}Lu($\alpha 3n$)	8.24 d	$7/2^+$	667.4	11.1
			739.8	47.9
^{172}Lu($\alpha 2n$)	6.7 d	4^-	900.7	29.8
			1093.6	63.0

TABLE II. List of identified reaction residues in the ^{9}Be + ^{187}Re reaction and their decay data [31,32].

Residue	$T_{1/2}$	J^π	E_γ (keV)	I_γ (%)
^{191}Au($5n$)	3.18 h	$3/2^+$	277.9	6.4
			283.9	5.9
			586.5	15.0
^{192}Au($4n$)	4.94 h	1^-	296.0	23.0
			316.5	59.0
^{193}Au($3n$)	17.65 h	$3/2^+$	255.6	6.2
^{189}Ir($\alpha 3n$)	13.2 d	$3/2^+$	245.1	6.0
^{190}Ir^{g} ($\alpha 2n$)	11.78 d	4^-	371.2	22.8
			528.6	34.0
			558.0	30.1
^{190} Ir^{m} ($\alpha 2n$)	3.09 h	11^-	616.5	90.1

the uncontaminated intense γ lines were chosen to evaluate the cross sections. The other γ lines corresponding to the same ERs were also used to cross-check the accepted cross-section values. The experimentally measured cross sections for the production of various residues populated in the ^{9}Be + ^{169}Tm and ^{9}Be + ^{187}Re systems are given in Tables III and IV, respectively. Errors in the measured ER cross sections include systematic uncertainties that could arise from different sources such as (i) target thickness (∼3%), (ii) beam current (∼3%), and (iii) detector efficiency (∼3%), and statistical error on γ-yield extraction. The systematic uncertainties are added in quadrature to the statistical error to get the total error in the cross section. It can be seen in Tables III and IV that the errors of the measured ER cross sections are mainly from the statistical uncertainties; namely, reaching a maximum of 49% at energy of 39.2 MeV for the residue ^{189}Ir due to its low cross section and low-intensity branching ratio.

Based on the assumption of the statistical model (SM), the branching ratios of individual channels with respect to the complete fusion depends only on the compound nucleus formed by complete fusion. Thus one can use the prediction of the statistical model to check and correct the measured cross sections. In the present work, the relative contributions of measured cross sections for neutron evaporation channels to CF have been compared with statistical model calculations performed using the code PACE2 [33]. In the SM calculations, the default optical potentials available in PACE2 were used, while the l distribution obtained from the FRESCO [34] calculations was fed as an input at each energy to obtain the cross sections. One important parameter in the SM calculations is the level density a, which is calculated from the expression $a = A/K$ MeV^{-1}, where A is the nucleon number of a compound system and K is a free parameter. The branching ratios of $\sigma_{xn}/\Sigma\sigma_{xn}(x = 3, 4, 5)$ were calculated with different level-density parameters K from 9 to 13. The calculations with $K = 13$ and 10, respectively, for ^{9}Be + ^{169}Tm and ^{9}Be + ^{187}Re systems, were found to provide a good description of the present experimental data over a broad energy range. The results of PACE2 calculations as well as experimental data for these two systems are shown in Figs. 7 and 8, respectively. If we

TABLE III. Measured cross sections for the production of various residues, ICF, and CF (corrected by PACE2) along with the ratio R (see text for definition) for the ^{9}Be + ^{169}Tm reaction. The nominal Coulomb barrier, using the Sao Paulo potential [35], is 35.4 MeV at the laboratory. The notation is such that αxn means the evaporation of xn after the fusion of α with the target.

E_{lab} (MeV)	^{173}Ta ($5n$) (mb)	^{174}Ta ($4n$) (mb)	^{175}Ta ($3n$) (mb)	^{171}Lu ($\alpha 3n$) (mb)	^{172}Lu ($\alpha 2n$) (mb)	$\sigma^{expt}_{3n+4n+5n}$ (mb)	σ_{ICF} (mb)	R	σ^{expt}_{CF} (mb)	CF/TF
48.0	66.0 ± 4.1	642.3 ± 58.0	50.1 ± 3.3	131.8 ± 7.6	122.5 ± 7.1	758.4 ± 65.4	254.3 ± 14.7	0.930	815.1 ± 70.3	0.76
46.9	29.2 ± 2.5	594.2 ± 39.3	59.3 ± 3.6	114.5 ± 6.5	135.0 ± 7.4	682.7 ± 45.4	249.5 ± 13.9	0.934	730.8 ± 48.6	0.75
45.7	11.9 ± 1.3	507.5 ± 43.0	80.8 ± 5.1	90.3 ± 5.3	139.0 ± 7.7	600.1 ± 49.4	229.3 ± 13.0	0.941	638.0 ± 52.5	0.74
44.5		407.1 ± 30.8	91.9 ± 6.3	55.7 ± 3.6	126.2 ± 7.2	499.0 ± 37.1	181.9 ± 10.8	0.945	527.8 ± 39.3	0.74
43.2		292.5 ± 25.0	120.8 ± 7.0	38.8 ± 2.2	137.8 ± 7.7	413.2 ± 32.0	176.6 ± 9.9	0.950	435.2 ± 33.7	0.71
42.0		195.5 ± 19.1	137.2 ± 7.8	23.8 ± 1.6	132.1 ± 7.3	332.7 ± 26.9	155.9 ± 8.9	0.955	348.3 ± 28.8	0.69
40.2		111.3 ± 16.4	136.0 ± 7.8	12.4 ± 0.8	110.8 ± 7.2	247.2 ± 24.2	123.2 ± 8.0	0.959	257.9 ± 25.3	0.68
38.9		49.0 ± 6.3	129.6 ± 8.6	4.7 ± 0.4	95.1 ± 5.4	178.6 ± 14.9	99.8 ± 5.8	0.961	185.9 ± 15.5	0.65
37.7		15.4 ± 2.1	99.1 ± 5.9	2.1 ± 0.5	67.8 ± 3.9	114.5 ± 8.0	69.9 ± 4.4	0.958	119.5 ± 8.4	0.63
36.3		2.4 ± 0.6	54.1 ± 3.4		40.9 ± 2.3	56.4 ± 4.0	40.9 ± 2.3	0.962	58.6 ± 4.2	0.59
35.0			20.8 ± 1.9		17.3 ± 1.0	20.8 ± 1.9	17.3 ± 1.0	0.953	21.8 ± 2.0	0.56
33.5			3.3 ± 0.5		4.5 ± 0.3	3.3 ± 0.5	4.5 ± 0.3	0.970	3.4 ± 0.5	0.43
32.1					1.2 ± 0.2		1.2 ± 0.2			

vary the values of K within the range from 9 to 13, the results do not change too much, although the fits get a bit worse.

By using the same parameters in PACE2, the missing ER contributions to the total CF have been corrected by taking the ratio $R = \sigma^{PACE2}_{3n+4n+5n}/\sigma^{PACE2}_{CF}$ and using this ratio to calculate the CF cross sections by $\sigma^{expt}_{CF} = \sigma^{expt}_{3n+4n+5n}/R$. The values of the ratio R and the fusion cross sections σ^{expt}_{CF} obtained are given in Tables III and IV. As listed in Tables III and IV, the summed cross sections of $3n$, $4n$, and $5n$ channels predicted by PACE2 are found to be in the range of 92 to 97% of CF for ^{9}Be + ^{169}Tm reaction and 98 to 99% of CF for the ^{9}Be + ^{187}Re reaction.

This small correction does not change significantly if different values of level-density parameters are used, corresponding to no more than 2% to 3% in the uncertainty of the fusion cross sections. This can be observed in Fig. 9, which shows the correction ratios as a function of energy, for the two systems, when the values of K are changed from 9 to 13.

It is important to mention that, although the residues of $\alpha 2n$ and $\alpha 3n$ channels, as listed in Tables III and IV, might arise from both CF and/or ICF processes, where the former is the complete fusion of ^{9}Be with target followed by the evaporation of one α and two or three neutrons, the evaporation code PACE2 predicts that the CF compound nuclei formed in ^{9}Be + ^{169}Tm and ^{9}Be + ^{187}Re systems decay overwhelmingly by neutron evaporation, and the total of evaporation of α channels is less than 2% and 0.5%, respectively, in two systems. Therefore, the sum of $\alpha 2n$ and $\alpha 3n$ channels was used, in the present work, to determine the ICF cross sections, separated from the CF. This is not the situation for lighter systems, where the evaporation of charged particles is important and that is the main reason why there is no reported experimental determination of CF and ICF for light systems, but rather only TF. On the other hand, in the reported experimental determinations of fusion of ^{9}Be (see, for example Refs. [20,23,24]), it is assumed that CF is

TABLE IV. Measured cross sections for the production of various residues, ICF and CF (corrected by PACE2) along with the ratio R (see text for definition) for the ^{9}Be + ^{187}Re reaction. The nominal Coulomb barrier, using the Sao Paulo potential [35], is 37.6 MeV at the laboratory. The notation is such that αxn means the evaporation of xn after the fusion of α with the target.

E_{lab} (MeV)	^{191}Au ($5n$) (mb)	^{192}Au ($4n$) (mb)	^{193}Au ($3n$) (mb)	^{189}Ir ($\alpha 3n$) (mb)	^{190}Ir ($\alpha 2n$) (mb)	$\sigma^{expt}_{3n+4n+5n}$ (mb)	σ_{ICF} (mb)	R	σ^{expt}_{CF} (mb)	CF/TF
49.1	201.7 ± 11.5	458.8 ± 28.6	1.9 ± 0.5	115.1 ± 9.1	96.9 ± 6.2	662.3 ± 40.6	212.0 ± 15.3	0.987	671.1 ± 41.1	0.76
48.1	137.1 ± 8.4	462.9 ± 27.2	3.6 ± 1.1	78.9 ± 10.3	97.9 ± 6.7	603.6 ± 36.7	176.8 ± 17.0	0.988	610.9 ± 37.1	0.78
47.2	88.5 ± 5.5	477.3 ± 29.9	6.9 ± 2.0	68.1 ± 12.9	104.4 ± 6.5	572.7 ± 37.4	172.4 ± 19.4	0.989	579.1 ± 37.8	0.77
46.2	43.0 ± 4.9	419.4 ± 24.2	12.5 ± 2.3	75.8 ± 10.1	95.3 ± 6.2	475.0 ± 31.4	171.1 ± 16.3	0.990	479.8 ± 31.7	0.74
45.0	13.3 ± 1.5	373.0 ± 21.6	17.7 ± 2.6	49.5 ± 8.8	96.2 ± 6.5	404.0 ± 25.7	145.8 ± 15.3	0.991	407.7 ± 25.9	0.74
44.0		329.0 ± 18.1	20.3 ± 6.3	36.9 ± 9.6	106.3 ± 6.5	349.3 ± 24.4	143.2 ± 16.1	0.991	352.5 ± 24.6	0.71
42.7		259.3 ± 14.4	21.1 ± 3.4	20.4 ± 3.3	100.7 ± 6.1	280.4 ± 17.8	121.1 ± 9.4	0.992	282.7 ± 17.9	0.70
40.3		104.1 ± 5.7	31.6 ± 5.2	14.6 ± 5.4	80.9 ± 5.4	135.7 ± 10.9	95.5 ± 10.8	0.994	136.6 ± 11.0	0.59
39.2		62.8 ± 3.9	28.4 ± 3.8	7.0 ± 3.4	60.2 ± 3.9	91.3 ± 7.7	67.2 ± 7.3	0.993	91.9 ± 7.8	0.58
38.0		22.6 ± 1.6	23.1 ± 2.8		37.9 ± 3.0	45.7 ± 4.4	37.9 ± 3.0	0.993	46.0 ± 4.4	0.55
36.8		5.0 ± 0.4	9.8 ± 2.7		17.4 ± 1.4	14.8 ± 3.1	17.4 ± 1.4	0.993	14.9 ± 3.1	0.46
35.5		0.9 ± 0.3	4.6 ± 0.8		6.3 ± 0.8	5.4 ± 1.1	6.3 ± 0.8	0.990	5.5 ± 1.1	0.47
34.2					2.4 ± 0.6		2.4 ± 0.6			

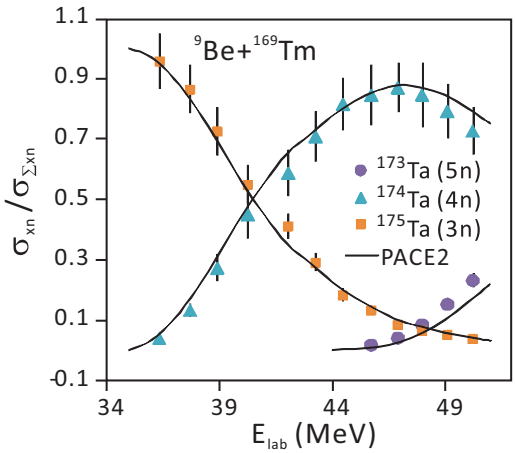

FIG. 7. (Color online) Experimental and predicted ratios of a given complete fusion xn evaporation product to the sum of all such products for the ^{9}Be + ^{169}Tm reaction. In PACE2 calculations, the level-density parameter $K = 13$ was used.

the fusion of the total charge of the projectile, that is, the sum of fusion cross sections of ^{9}Be and ^{8}Be with the target. In our present work, we also make the same assumption. However, the very good agreement of our derived evaporation cross sections, supposing that only ^{9}Be fuses, with PACE2 predictions may be considered as a signature that the fusion cross section of ^{8}Be is negligible when compared with the ^{9}Be cross section.

IV. COMPARISON OF FUSION DATA WITH COUPLED-CHANNEL CALCULATION PREDICTIONS

In order to compare the CF and TF cross section data with theoretical predictions, we performed the usual coupled-channel (CC) calculations without taking into account breakup and transfer channels. Thus, we expect that the differences between theoretical predictions and experimental results are due to coupling effects of the channels not included in

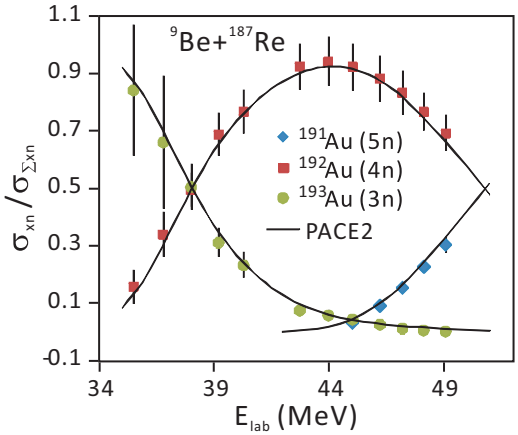

FIG. 8. (Color online) Experimental and predicted ratios of a given complete fusion xn evaporation product to the sum of all such products for the ^{9}Be + ^{187}Re reaction. In PACE2 calculations, the level-density parameter $K = 10$ was used.

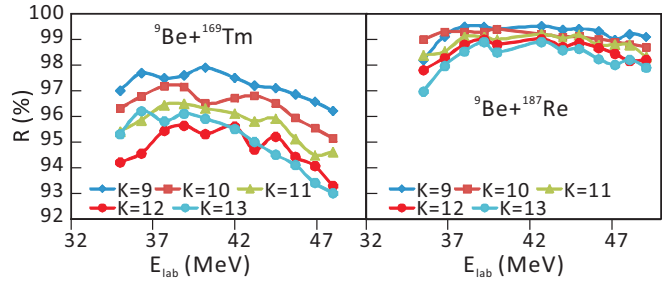

FIG. 9. (Color online) Correction ratios ($R = \sigma^{\mathrm{PACE2}}_{3n+4n+5n}/\sigma^{\mathrm{PACE2}}_{\mathrm{CF}}$) as a function of energy, for the two studied systems, when the values of K are changed from 9 to 13.

calculations. Actually, recently Jha *et al.* [17] performed CC calculations for fusion of ^{9}Be on some targets, including the one-neutron channel, and the results showed that the effect of the transfer channel on fusion was negligible. So, we will assume that the differences between theory and data are due to dynamical breakup effects on fusion.

In this kind of calculation, it is very important to adopt a reliable bare potential. It was recently shown that the choice of the optical potential used for coupled-channel calculations plays an upmost role, and that the conclusions of the effect of breakup channels on fusion cross sections at different energy regimes may strongly depend on the bare potential used in coupled-channel calculations [36]. For this reason we chose the parameter-free double-folding bare Sao Paulo potential (SPP) [35], which uses realistic densities and has no free parameters, as the bare potential. In the coupled-channel calculations, we included only the inelastic excitations of the targets. No resonance in the continuum states of the ^{9}Be was included in the calculations, since this is already part of the breakup process, which is the object of the investigation. The ^{9}Be-ground-state deformation was not included. If we included this deformation, all results would slightly change towards a larger theoretical value and therefore a larger value of the suppression factor would be found. We checked the effect of the ground-state deformation by including it in the coupled-channel scheme. We found $\sim$10% as the largest effect for both systems at energies above the Coulomb barrier. Because the deformation of the ground state was not included for the other systems in the literature, we also did not include it in our final calculation. All coupled-channel calculations were performed with the FRESCO code [34].

For the ^{9}Be + ^{187}Re system, because the target is odd, the weak-coupling model was used for ^{187}Re. Thus, the ^{187}Re nucleus was considered as a ^{186}W core plus one extra proton, considered as a spectator when the core is excited to its collective ground-state rotational band. The excitations up to the 6^{+} state of the core were considered in the calculations. The quadrupole deformation parameter $\beta_2 = 0.226$ was taken from Ref. [37], and the same value was assumed for nuclear and Coulomb deformations. For the real part of the optical potential the Sao Paulo potential was used [35]. For the imaginary part of the optical potential, although not all relevant channels were considered in the coupled-channel calculations, we used a Woods–Saxon potential internal to the Coulomb barrier to

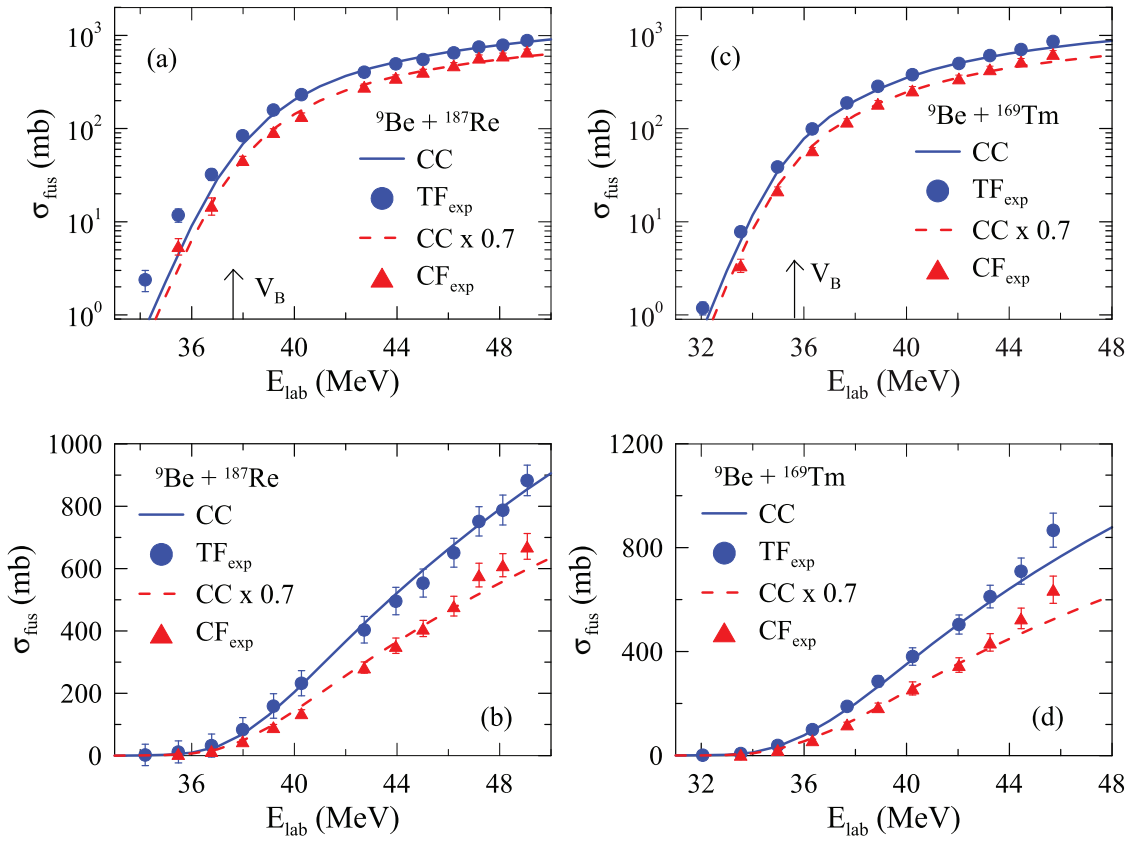

FIG. 10. (Color online) Comparison of the experimental fusion excitation functions for the ^{9}Be + ^{187}Re (left panels) and ^{9}Be + ^{169}Tm (right panels) with coupled-channel calculations that do not include the breakup channel. See text for details.

account for the absorption of the flux that pass through or over the barrier (equivalent to the so-called ingoing-wave boundary condition [38,39]). The potential parameters were $W_0 = 50$ MeV, $r_0 = 1.06$ fm and $a = 0.2$ fm for the depth, reduced radius, and diffuseness, respectively. We checked that the fusion cross section does not depend on the choice of these parameters, as long as the imaginary potential remains internal to the Coulomb barrier. We would like to emphasize that, in reactions between a light projectile and a medium-heavy target, the effect of couplings above the Coulomb barrier is almost negligible. The energy region above the barrier is the one that we are mainly concerned with in the present work. At energies near and below the Coulomb barriers, some slight influence might be found due to our weak-coupling approximation for the excitation of the target. One solution to avoid our approximation would be to use a model-independent coupled-channels calculation by using the reduced transition probabilities among the target excited states. However, information in the literature is very scarce about the reduced electromagnetic transition probabilities for the ^{187}Re nucleus. In Figs. 10(a) and 10(b) we show the results of the calculations and the data for CF and TF in logarithmic and linear scales. The first is more suitable to observe the deviations at low and subbarrier energies, whereas the latter makes a zoom to observe the effects at energies above the barrier. From Fig. 10(b) we can observe that there is CF suppression of the order of 30% at energies above the barrier when compared with the theoretical predictions. The TF cross-section data are in agreement with the calculations, which indicates that the ICF seems to be the responsible for the loss of flux going to CF, and consequently suppressing the CF at this energy regime. On the other hand, from Fig. 10(a) one can observe a small enhancement of CF and TF at subbarrier energies, when compared with calculations.

In the coupled-channel calculations for the ^{9}Be + ^{169}Tm system the weak-coupling model was also used for the ^{169}Tm target. In this case the ^{169}Tm nucleus was considered as a ^{170}Yb core plus a proton hole, considered as a spectator when the core is excited to its collective ground-state rotational band. The excitations up to the 4^+ state of the core were considered in the calculations. The higher-spin members of the rotational band produced instabilities in the calculations, and almost no effect in the calculated fusion cross section. For these reasons they were neglected in the final calculations. The quadrupole deformation parameter $\beta_2 = 0.326$ was taken from Ref. [37], and the same value was assumed for nuclear and Coulomb deformations. In Figs. 10(c) and 10(d) we show the results for this system, also in logarithmic and linear scales. The results are similar to those for the ^{9}Be + ^{187}Re system, and the suppression of CF at energies above the barrier is also found to be of 30%.

We can make a "zoom" in Fig. 10 and compare CF data for the two systems with the coupled-channel calculations by plotting the CF suppression factor for each system. This

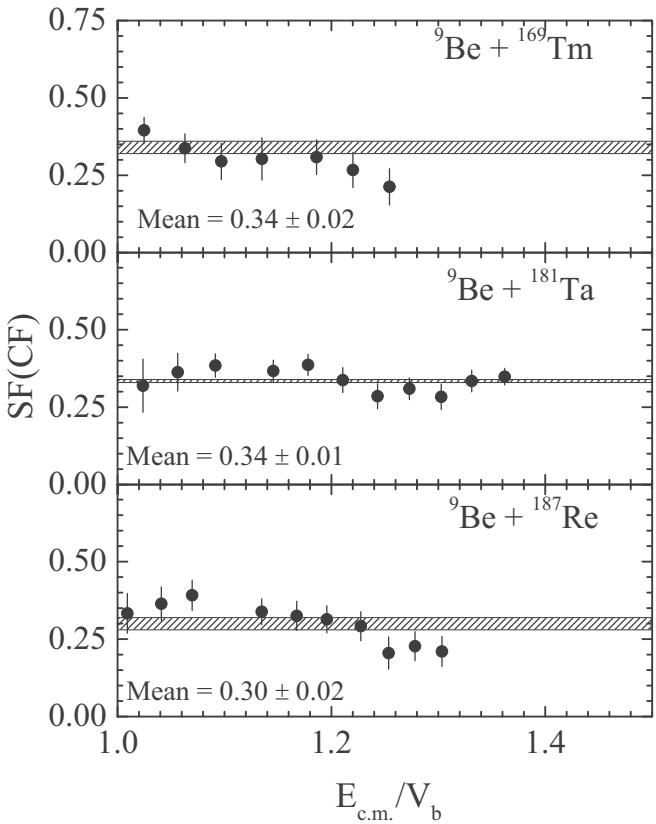

FIG. 11. Complete fusion suppression factor as a function of the energy, as compared with predictions from coupled-channel calculations. See text for details.

quantity is defined as SF(CF) $= 1 - y$, where y is the factor with which the results of the CC calculations have to be multiplied in order to agree with the CF data. The results are shown in Fig. 11, where we also included the ^{9}Be + ^{181}Ta system, measured recently by our group [20]. We can observe that, in the energy region just above the barrier, the average suppression is indeed of the order of 30%.

V. SYSTEMATICS OF RESULTS FOR FUSION OF ^{9}BE

In this section we investigate a possible systematic behavior of the CF excitation functions for fusion induced by ^{9}Be. Together with the two systems measured in the present work, there are seven other measured systems reported in literature for the ^{89}Y, ^{124}Sn, ^{144}Sm, ^{181}Ta, ^{186}W, ^{208}Pb, and ^{209}Bi targets [14,18–24]. We do not include in the discussion the light ^{27}Al and ^{64}Zn and the heavy ^{238}U targets [25–28] because, for those systems, only TF cross sections were measured. Table V shows a summary of the available data for CF of ^{9}Be-induced fusion reactions, including the energy range of the measurements and the percentage of the fusion cross sections that could be determined experimentally, following the predictions of the PACE2 code [33]. For the ^{9}Be + ^{89}Y, ^{124}Sn, and ^{209}Bi, ICF was not measured.

Our first approach is to try to obtain a model-independent systematic for the CF/TF ratio for each of the six systems

TABLE V. Summary of the available data for CF of ^{9}Be-induced fusion reactions, where V_B is the Coulomb-barrier energy in the center-of-mass frame.

Target	Energy range $E_{c.m.}/V_B$	CF (%) measured	V_B (MeV)	Reference
^{89}Y	0.82–1.36	80%–90%	21.1	[18]
^{124}Sn	0.91–1.35	88%–95%	25.6	[14]
^{144}Sm	0.91–1.33	97%–98%	31.1	[19]
^{169}Tm	0.90–1.28	92%–97%	33.6	Present work
^{181}Ta	0.95–1.35	98%–99%	35.2	[20]
^{186}W	1.19–1.54	100%	35.4	[21]
^{187}Re	0.88–1.33	99%	35.9	Present work
^{208}Pb	0.88–1.27	100%	38.5	[22–24]
^{209}Bi	1.09–1.48	100%	38.8	[22]

for which this ratio could be determined experimentally. We restrict the analysis of the CF/TF ratio to energies above the Coulomb barrier, because at lower energies, especially at subbarrier energies, this ratio increases owing to the large contribution of direct stripping transfer reactions like ^{4}He, ^{5}He, and sequential one-neutron followed by α transfer from ^{8}Be. As is well known, at subbarrier energies transfer cross sections are larger than fusion cross sections, since they do not need to tunnel through the barrier. Therefore, what one (ourselves and other authors [14,18–24]) calls ICF at this regime is, actually, transfer plus ICF, with predominance of the first. As shown in Fig. 12, one can observe that, for four of the six systems, the average ratios in this energy region are between 0.30 and 0.34, which could be considered as target independent, when one considers the error bars. For the ^{144}Sm and ^{186}W systems, this ratio is smaller. The differences between Figs. 11 and 12 are that the latter is model independent and requires the measurement of both CF and ICF, what is available for only six of the nine systems.

Our second approach to investigate the ^{9}Be CF cross section systematic behavior is to compare CF data for all systems in the same plot by using the benchmark universal fusion function (UFF) curve [5]. The dimensionless function $F(x)$, called the fusion function, is defined as $F(x) = (2E_{c.m.}\sigma_{fus})/(R_B^2\hbar\omega)$. The (UFF) is $F_0(x) = \ln[1 + \exp(2\pi x)]$, where $x = [E_{c.m.} - V_B)/(\hbar\omega)]$, with V_B, R_B, and $\hbar\omega$ being the height, radius, and the curvature of the Coulomb barrier. The UFF is a universal and benchmark curve for any system when plotted versus the quantity x. In Fig. 13 we plot the CF fusion function for seven of the nine systems investigated and the UFF curve. The ^{9}Be + ^{144}Sm and ^{186}W seem to be out the systematics and deserve further investigation. The points are the experimental CF functions, renormalized to take into account the effects of the couplings of inelastic excitations of the targets, as explained in details by Canto *et al.* [5]. The difference between the points and the UFF curve is the observed effect of the breakup of ^{9}Be on the CF for all systems. One can observe that for all systems, the data are within the range of the UFF curve multiplied by 0.65 to 0.75, which means CF suppression from 25% to 35%. This result is in agreement with a recently reported paper by Wang *et al.* [40], when an average 32% CF suppression was found, following a chi-square fit of the four

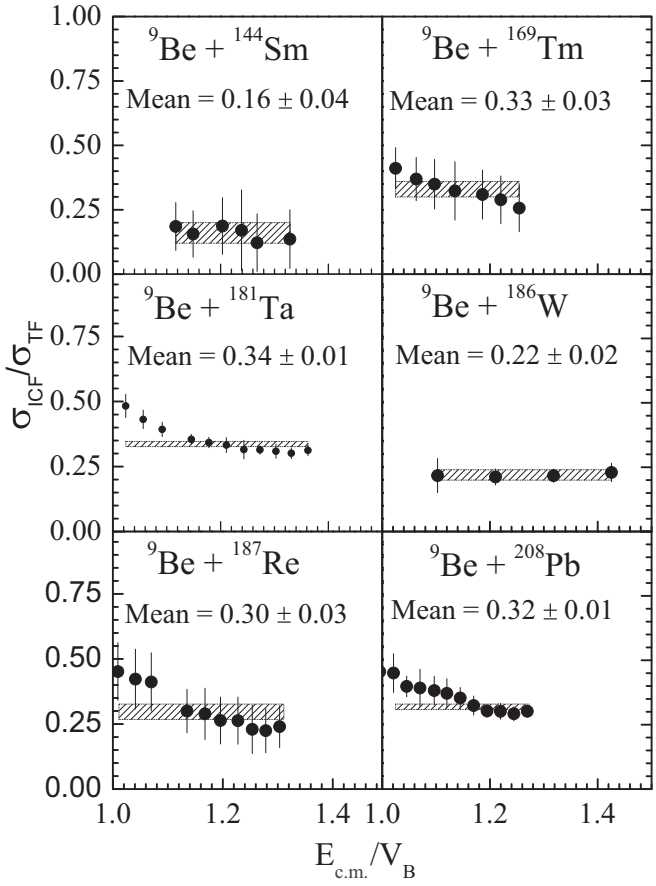

FIG. 12. Energy dependence of the ratio ICF/TF cross sections for energies slightly above the Coulomb barrier, for the six systems for which ICF and CF have been measured.

available systems at that time (they also left the ^{144}Sm and ^{186}W out of the fit procedure).

In Fig. 14 we show a similar figure, but for total fusion (TF), for five systems for which TF could be measured. Now

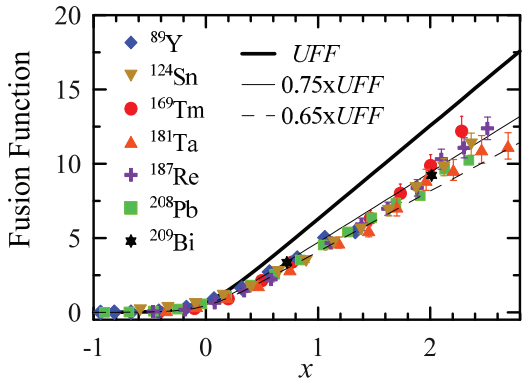

FIG. 13. (Color online) Complete fusion functions for ^{9}Be-induced fusion of several targets. The thick black curve is the benchmark UFF curve (see text for details). The two thin curves are the UFF curve multiplied by 0.75 and 0.65. All data are within these two curves, which means CF suppression of the order of 25% to 35%.

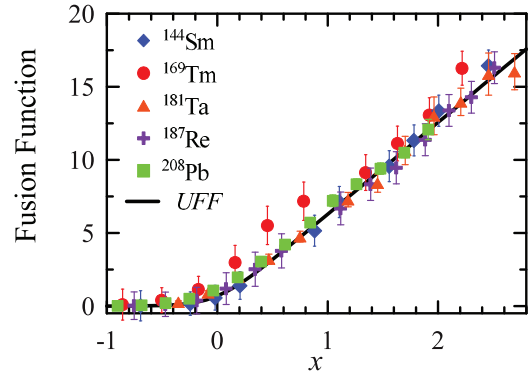

FIG. 14. (Color online) Total-fusion functions for ^{9}Be-induced fusion of several targets. The thick black curve is the benchmark UFF curve (see text for details). All data are in agreement with this curve, which means that there is no breakup effect on TF at this energy range.

we observe that there is no TF suppression due to the breakup coupling to fusion. Now, the ^{9}Be + ^{186}W system was left out of the systematic, since it is the only one for which some TF suppression is found.

Although it is out of the scope of the present paper, from the present results we might say a few words about the two systems which are out of the systematics. For the ^{144}Sm target, the CF suppression is found to be smaller than the systematics, although the TF behavior agrees with the other systems. A possible explanation might be that some events corresponding to ICF were considered as CF in the determination of the cross sections. Concerning the ^{186}W target, it seems that some ICF and CF cross sections are missing.

VI. CONCLUSIONS

We measured precise complete and incomplete fusion cross sections for the ^{9}Be + ^{169}Tm and ^{187}Re systems, at energies near the Coulomb barrier. The activation technique with the detection of offline γ rays was used to derive the cross sections. Complete fusion suppression of the order of 30% was found for both systems, at the energy range slightly above the Coulomb barrier. This suppression is found in relation to predictions of coupled-channels calculations that do not include the breakup channel. As we used a double-folding potential with realistic densities, this suppression is attributed to dynamic effects of the breakup and corresponds to the flux that, instead of going to fusion, actually goes to the incomplete fusion channel, where one α particle fragment of the projectile fuses with the target. Furthermore, we investigated a possible systematic behavior of the suppression of complete fusion cross sections for different targets available in literature. We found that the suppression is roughly independent of the target. As the breakup should increase with the target mass or charge, we suppose that most of the breakup is of the delayed kind that cannot affect fusion, whereas the prompt breakup effect on fusion does not depend on the target.

ACKNOWLEDGMENTS

The authors wish to thank the staffs of HIRFL for the operation of the cyclotron and friendly collaboration during the experiment. C.J. Lin, H.M. Jia and V.V. Parkar are gratefully acknowledged. P.R.S. Gomes also thanks the CUSTIPEN (China-U.S. Theory Institute for Physics with Exotic Nuclei), since his attendance at the workshop in Beijing helped him to go to Lanzhou to finish the present work. This work was supported by the National Natural Sciences Foundation (Grants No. U1232124, No. 10905075, and No. 11305221), the Major State Basic Research Development Program of China (Grant No. 2013CB834403), and the ADS project No. 302 (Y103010ADS) of the Chinese Academy of Sciences. P.R.S. Gomes and J. Lubian acknowledge partial support from CNPq, FAPERJ, and Pronex.

[1] L. F. Canto, P. R. S. Gomes, R. Donangelo, and M. S. Hussein, Phys. Rep. **424**, 1 (2006).
[2] J. F. Liang and C. Signorini, Int. J. Mod. Phys. E **14**, 1121 (2005).
[3] N. Keeley, R. Raabe, N. Alamanos, and J. L. Sida, Prog. Part. Nucl. Phys. **59**, 579 (2007).
[4] B. B. Back, H. Esbensen, C. L. Jiang, and K. E. Rehm, Rev. Mod. Phys. **86**, 317 (2014).
[5] L. F. Canto, P. R. S. Gomes, J. Lubian, L. C. Chamon, and E. Crema, J. Phys. G **36**, 015109 (2009); Nucl. Phys. A **821**, 51 (2009).
[6] R. Rafiei, R. du Rietz, D. H. Luong, D. J. Hinde, M. Dasgupta, M. Evers, and A. Diaz-Torres, Phys. Rev. C **81**, 024601 (2010).
[7] D. H. Luong, M. Dasgupta, D. J. Hinde, R. du Rietz, R. Raferi, C. J. Lin, M. Evers, and A. Diaz-Torres, Phys. Lett. B **695**, 105 (2011).
[8] D. H. Luong, M. Dasgupta, D. J. Hinde, R. du Rietz, R. Rafiei, C. J. Lin, M. Evers, and A. Diaz-Torres, Phys. Rev. C **88**, 034609 (2013).
[9] D. R. Otomar, P. R. S. Gomes, J. Lubian, L. F. Canto, and M. S. Hussein, Phys. Rev. C **87**, 014615 (2013).
[10] M. S. Hussein, P. R. S. Gomes, J. Lubian, D. R. Otomar, and L. F. Canto, Phys. Rev. C **88**, 047601 (2013).
[11] H. Kumawat *et al.*, Phys. Rev. C **86**, 024607 (2012).
[12] M. K. Pradhan *et al.*, Phys. Rev. C **83**, 064606 (2011).
[13] L. R. Gasques, D. J. Hinde, M. Dasgupta, A. Mukherjee, and R. G. Thomas, Phys. Rev. C **79**, 034605 (2009)
[14] V. V. Parkar *et al.*, Phys. Rev. C **82**, 054601 (2010).
[15] P. K. Rath *et al.*, Phys. Rev. C **79**, 051601(R) (2009).
[16] P. R. S. Gomes, R. Linares, J. Lubian, C. C. Lopes, E. N. Cardozo, B. H. F. Pereira, and I. Padron, Phys. Rev. C **84**, 014615 (2011).
[17] V. Jha, V. V. Parkar, and S. Kailas, Phys. Rev. C **89**, 034605 (2014).
[18] C. S. Palshetkar, S. Santra, A. Chatterjee, K. Ramachandran, S. Thakur, S. K. Pandit, K. Mahata, A. Shrivastava, V. V. Parkar, and V. Nanal, Phys. Rev. C **82**, 044608 (2010).
[19] P. R. S. Gomes *et al.*, Phys. Rev. C **73**, 064606 (2006); Phys. Lett. B **634**, 356 (2006).
[20] N. T. Zhang, Y. D. Fang, P. R. S. Gomes, J. Lubian, M. L. Liu, X. H. Zhou, G. S. Li, J. G. Wang, S. Guo, Y. H. Qiang, Y. H. Zhang, D. R. Mendes Junior, Y. Zheng, X. G. Lei, B. S. Gao, Z. G. Wang, K. L. Wang, and X. F. He, Phys. Rev. C **90**, 024621 (2014).
[21] Y. D. Fang *et al.*, Phys. Rev. C **87**, 024604 (2013).
[22] M. Dasgupta, D. J. Hinde, S. L. Sheehy, and B. Bouriquet, Phys. Rev. C **81**, 024608 (2010).
[23] M. Dasgupta *et al.*, Phys. Rev. Lett. **82**, 1395 (1999).
[24] M. Dasgupta *et al.*, Phys. Rev. C **70**, 024606 (2004).
[25] G. V. Marti *et al.*, Phys. Rev. C **71**, 027602 (2005).
[26] S. B. Moraes, P. R. S. Gomes, J. Lubian, J. J. S. Alves, R. M. Anjos, M. M. Sant'Anna, I. Padrón, C. Muri, R. Liguori Neto and N. Added, Phys. Rev. C **61**, 064608 (2000).
[27] P. R. S. Gomes *et al.*, Phys. Lett. B **601**, 20 (2004).
[28] R. Raabe, C. Angulo, J. L. Charvet, C. Jouanne, L. Nalpas, P. Figuera, D. Pierroutsakou, M. Romoli, and J. L. Sida, Phys. Rev. C **74**, 044606 (2006).
[29] G. Scheidenberger and H. Geissel, Nucl. Instrum. Methods Phys. Res., Sect. B **135**, 25 (1985).
[30] D. Bazin, O. Tarasov, M. Lewitowicz, and O. Sorlin, Nucl. Instrum. Methods Phys. Res., Sect. A **482**, 307 (2002).
[31] R. B. Firestone, V. S. Shirley, C. M. Baglin, S. Y. Frank Chu, and J. Zipkin, *Table of Isotopes* (Wiley, New York, 1996).
[32] ENSDF-National Nuclear Data Center, BNL, USA; http://www.nndc.bnl.gov/ensdf/
[33] A. Gavron, Phys. Rev. C **21**, 230 (1980).
[34] I. J. Thompson, Comput. Phys. Rep. **7**, 167 (1988).
[35] L. C. Chamon, D. Pereira, M. S. Hussein, M. A. Candido Ribeiro, and D. Galetti, Phys. Rev. Lett. **79**, 5218 (1997); L. C. Chamon *et al.*, Phys. Rev. C **66**, 014610 (2002).
[36] L. F. Canto, P. R. S. Gomes, J. Lubian, D. R. Otomar, M. S. Hussein, and P. Lotti, Eur. Phys. J. A **50**, 89 (2014).
[37] S. Raman, C. W. Nestor Jr. and P. Tikkanem, At. Data Nucl. Data Tables **78**, 1 (2001).
[38] N. Oda and K. Harada, Prog. Theor. Phys. **15**, 545 (1956).
[39] G. Rawitscher, Phys. Rev. **135**, B605 (1964).
[40] B. Wang, W. J. Zhao, P. R. S. Gomes, E. G. Zhao, and S. G. Zhou, Phys. Rev. C **90**, 034612 (2014).